

Onset of flow in a confined colloidal glass under an imposed shear stress

Pinaki Chaudhuri^{1,2} and Jürgen Horbach¹

¹*Institut für Theoretische Physik II, Heinrich-Heine-Universität Düsseldorf, 40225 Düsseldorf, Germany*

²*Johannes-Gutenberg-Universität Mainz, Institut für Physik, WA 331, 55099 Mainz, Germany*

A confined colloidal glass, under the imposition of a uniform shear stress, is investigated using numerical simulations. Both at macro- and micro-scales, the consequent dynamics during the onset of flow is studied. When the imposed stress is gradually decreased, the time-scale for the onset of steady flow diverges, associated with long-lived spatial heterogeneities. Near this yield-stress regime, persistent creep in the form of shear-banded structures is observed.

PACS numbers:

A defining mechanical property of amorphous solids is the existence of a yield stress; these materials yield only when the applied stress exceeds this threshold [1]. In experiments, the material's yielding response is commonly probed by using stress as a control parameter [2]. Such measurements report about existence of a creeping regime, where the material deforms very slowly. In soft amorphous materials (e.g. colloids, gels, emulsions etc.), steady flow is often not observed in such situations within experimental durations [3, 4]. This is related to recent recognition of diverging time-scales for the onset of flow [5–7]. Beyond these macro-measurements, little is known about the spatio-temporal characteristics of the local dynamics around yielding, which would allow for improved understanding of the micro-mechanisms at play.

An emerging scenario for the micro-dynamics is that when the material is sheared, structural rearrangements occur locally [8–10] which subsequently trigger more events nearby and this correlated process initiates and sustains the flow. Kinetic elastoplastic models [11] based on such a picture of fluidization have been able to explain various steady-state flow properties in confined systems [12–14]. Further, it has been conjectured that the triggering process results in an avalanche-like behaviour, as evidenced via simulations [15, 16]. Here, we focus on such micro-macro processes when a quiescent glass is subjected to an external stress. Recent creep measurements in a carbopol gel [5] as well as in a granular mixture [17, 18] indicate that in those materials flow occurs via the formation of local plastic events which build up to form transient shear-bands. However, whether these flow inhomogeneities are generic to the fluidization of amorphous systems under imposed stresses and linked to the correlated processes discussed above, needs clarification.

In this Letter, we report a simulational study of a confined colloidal glass under an imposed *uniform shear stress* to elucidate the nature of the local dynamics during the *onset of flow*. We use a geometry that mimics the typical planar Couette setup in stress-controlled experiments of soft materials. We show that indeed the time-scale for the onset of steady flow diverges when the stress is decreased, along with the emergence of nonlinear creep (similar to a range of materials [5, 7, 19–22]). More-

over, by following the local dynamics, we observe that the mobility can be spatio-temporally heterogeneous and the mobile regions take the shape of shear-band-like structures. These structures have a lifetime which increases with decreasing stress, which is linked to the delayed onset of steady flow. Thus, our work provides evidence that in the presence of an external shear stress, the fluidization of the glass near yielding is extremely slow, along with the presence of persistent spatial heterogeneities.

In our simulations, we consider the model colloidal system of a 50 : 50 binary Yukawa fluid (for details of interactions and model parameters, see [23, 24]). Our molecular dynamics simulations have been done for samples consisting of $N = 12800$ particles, having the dimensions $L_x = 26.66 d_s$, $L_y = 53.32 d_s$, $L_z = 13.33 d_s$ (d_s is the diameter of the smaller particles). We work in the NVT ensemble and the temperature control is done by using a Lowe thermostat [25]. At a high temperature of $T = 0.2$, we equilibrated the system using periodic boundary conditions. Then, $m = 24$ independent configurations sampled at $T = 0.2$ were instantaneously quenched to $T = 0.05$ (below the mode-coupling critical temperature of $T_c = 0.14$ [23]). Each of these m configurations are then aged for durations of $t_{\text{age}} = 10^3, 10^4, 10^5$. When each configuration reaches a certain t_{age} , we freeze the particles at $0 < y < 2d_s$ and $L_y - 2d_s < y < L_y$ to prepare glassy states confined between rough walls. Then, these confined samples are sheared by pulling the top plate in $+x$ direction with a fixed force F_0 (similar to rheometers) [26], which imposes a constant shear stress of $\sigma_0 = F_0/[L_x L_z]$; we study the response of the confined glass to such a field.

Similar to experimental creep measurements, we study the response of the glass by monitoring the strain experienced at the top wall $\gamma_w(t)$. This is done by recording, for each of the m samples, the velocity of the wall $v_w(t)$ as a function of time, and then the average effective strain at the wall is obtained: $\gamma_w(t) = \langle \gamma_\alpha(t) \rangle_e$, where $\gamma_\alpha(t) = \int_0^t [v_w(t)/(L_y - 4d_s)] dt$ is the wall strain computed for α -th sample and $\langle \rangle_e$ is an average over the ensemble of m trajectories. In Fig. 1(a), we show how $\gamma_w(t)$ evolves for a wide range of imposed stress σ_0 . These

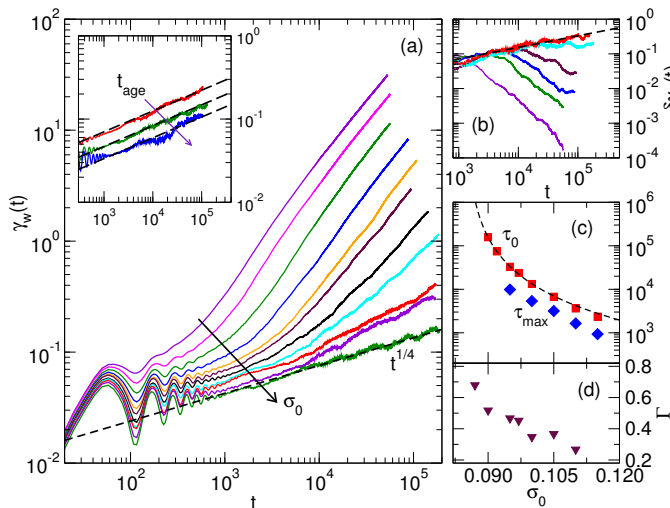


FIG. 1: (a) Evolution of strain at wall, $\gamma_w(t)$ for a range of imposed stress, $\sigma_0 = 0.115, 0.110, 0.105, 0.100, 0.097, 0.095, 0.092, 0.090, 0.087, 0.085, 0.080$ (from top to bottom), at $t_{\text{age}} = 10^4$. (Inset) $\gamma_w(t)$ at $\sigma_0 = 0.08$ at different ages ($t_{\text{age}} = 10^3, 10^4, 10^5$), with dashed lines corresponding to power law fits $\gamma_w(t) \sim t^{1/4}$. (b) Strain fluctuations across trajectories ($\delta\gamma_w(t)$) for different σ_0 ; the dashed line being a fit with $t^{1/3}$. (c) Variation with σ_0 : (In squares) Timescale (τ_0) to reach $\gamma_w = 1$; the dashed line is a fit with $A/(\sigma_0 - \sigma_s)^\beta$ ($\sigma_s = 0.0848$, $\beta = 2.285$). (In diamonds) Timescale (τ_{max}) at which the peak in $\delta\gamma_w(t)$ occurs. (d) With changing σ_0 , fluctuations in timescales (Γ) to reach strain of 0.3.

curves show several regimes - (i) in all cases, at early times, the strain increases initially and then there is an oscillatory part, corresponding to the regime when the stress builds up inside the confined sample - the oscillations occur due to the interplay of the imposed stress at the wall and the restoring force of the deformed glass; (ii) after this, for large values of σ_0 , one quickly sees an asymptotic linear regime in $\gamma_w(t)$, which corresponds to a steady flow at a fixed shear-rate; (iii) as σ_0 is decreased, an intermediate regime in $\gamma_w(t)$ emerges, which for small enough σ_0 has a power-law behaviour - for the creep at $\sigma_0 = 0.080$ (i.e. below the dynamic yield stress $\sigma_d = 0.0857$ [27]), we obtain a power-law exponent of 0.25. We also observe that the underlying process responsible for creep is not dependent on the age of the samples. In the inset of Fig. 1(a), we show the strain data for the different ages ($t_{\text{age}} = 10^3, 10^4, 10^5$): for all the three different ages, the exponent of the power law remains the same.

For most values of $\sigma_0 > \sigma_d$, one eventually observes the steady flow ($\gamma_w(t) \sim t$). One can define a time-scale for onset of flow, τ_0 , as the time required for the system to reach a strain of $\gamma_w(\tau_0) = 1$; using this definition, we calculate τ_0 for each σ_0 and plot it in Fig. 1(c) (squares). One can see that the time-scales increase with decreasing stress and the data can be fitted with the function

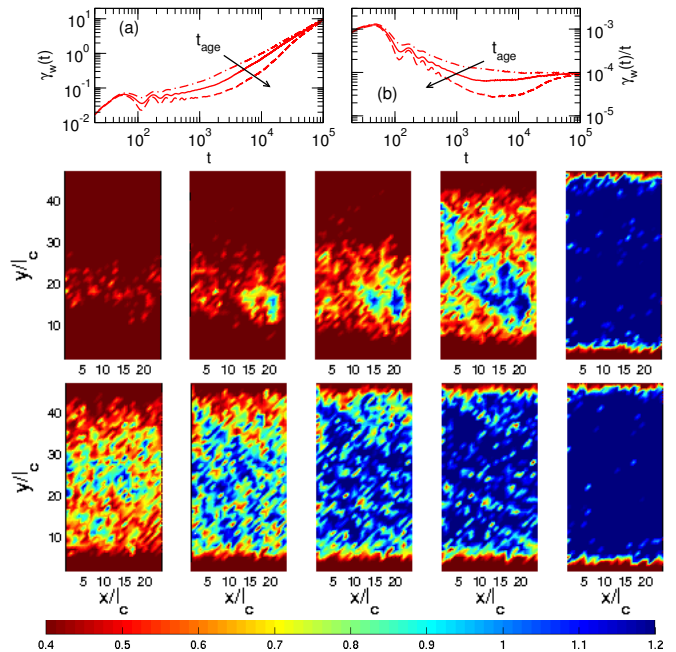


FIG. 2: *Top panel:* (a) Wall-strain $\gamma_w(t)$ for samples having different ages ($t_{\text{age}} = 10^3, 10^4, 10^5$) for imposed stress of $\sigma_0 = 0.1$. (b) Corresponding effective strain-rates, $\gamma_w(t)/t$ at the wall. *Middle panel:* Displacement maps for $t = 7470, 14940, 22410, 29880, 85905$ (from left to right) at a trajectory from $t_{\text{age}} = 10^5$ ensemble. *Bottom panel:* Maps at same times for a trajectory from $t_{\text{age}} = 10^3$ ensemble.

$A/(\sigma_0 - \sigma_s)^\beta$, with $\sigma_s = 0.0848$ ($\approx \sigma_d$, the estimated dynamical yield stress) and $\beta = 2.285$ (which is similar to experimental observations [5, 7]).

In supercooled liquids, diverging time-scales are seen to be associated with increasing heterogeneity in the dynamics [28]. For the onset of flow in glasses, we explore this possibility by studying the fluctuations in response within the ensemble of m samples having the same age; this is quantified by calculating $\delta\gamma_w(t) = \langle \gamma_\alpha^2(t) \rangle_e / \langle \gamma_\alpha(t) \rangle_e^2 - 1$. In Fig. 1(b), we plot $\delta\gamma_w(t)$ for different σ_0 . We see that for large values of σ_0 , the function $\delta\gamma_w(t)$ increases with time, has a maximum and then decays at long times. The initial increase in $\delta\gamma_w(t)$ has a power-law behaviour, which is identical for all σ_0 . This is similar to what was earlier observed in experiments of creep flow using paper samples [22] - a power-law in average strain, as well as a power law in the fluctuations. We can also track the location of the peak (τ_{max}) in $\delta\gamma_w(t)$; the variation of τ_{max} with σ_0 is shown in Fig. 1(c) - one can see that the increasing trend is similar to that for τ_0 . τ_{max} approximately corresponds to a macroscopic strain of $\gamma_w \sim 0.3$ as well as the time-scale at which diffusion sets in. Thus, the diverging time-scale for the onset of steady motion of the wall is linked to the increasing delay in the onset of diffusion within the system.

Till now, by monitoring the motion of the top wall, we have gauged the macroscopic response of the mate-

rial. We now want to see how deformation shapes up at a more local scale within the sample; whether the local response is uniform or heterogeneous and whether any spatial structures are formed as the system yields. In order to study this, we construct maps of transverse displacements (which are non-affine motions occurring due to the local structural rearrangements) in the following manner. Before we apply the external stress ($t = 0$), we divide the xy plane of the simulation box into small square cells (of length $l_c = 1.1 d_s$) and identify the particles in each cell. Next, after time t , we calculate the transverse displacement of each particle $\Delta y_i(t) = |y_i(t) - y_i(0)|$ and then calculate for each cell the local mobility, $\mu_{lm}(t) = \langle \Delta y_i(t) \rangle_{lm}$, where $\langle \rangle_{lm}$ is the average over all the particles in the cell $\{lm\}$ at $t = 0$, to construct the spatial maps.

We begin by using such maps to study the local dynamics for different ages of the samples, at a fixed imposed stress. For $\sigma_0 = 0.1$, the evolution of the macroscopic strain $\gamma_w(t)$ for trajectories at $t_{\text{age}} = 10^3, 10^4, 10^5$ as well as the corresponding effective strain-rates at the wall, $\gamma_w(t)/t$, are shown in Fig. 2(a) and 2(b), respectively. We see that the curvature in $\gamma_w(t)/t$ changes with age – while the curve for $t_{\text{age}} = 10^5$ has a pronounced minimum, it is a monotonically decreasing function for $t_{\text{age}} = 10^3$. This implies that the intermediate flow states could vary for samples having different ages. This we demonstrate via the mobility maps. The time evolution of local mobilities for a trajectory belonging to the ensemble with $t_{\text{age}} = 10^5$ is displayed in the middle panel of Fig. 2 (with the time increasing from left to right). The most important observation is that the transient local mobilities are spatially heterogeneous. Initially, a few spots of mobility evolve to a growing domain of large displacement. This then triggers mobility in the neighbourhood to form a structure which looks like a shear-band (spanning the length of the simulation box). This band then grows transversely as the mobility spatially spreads and eventually the entire system is fluidized. One can contrast this with the spatial mobilities for a trajectory from the ensemble with $t_{\text{age}} = 10^3$ (bottom panel of Fig. 2). Unlike the aged sample, here the spatial spread of large mobilities is quite uniform and it continues to be the case as the entire system gets eventually fluidized. Thus, the displacement maps clearly reveal that the transient flow states differ with aging [29]: for the more aged initial structure, an extended time window exists over which shear-banding is observed before the system finally becomes fully fluidized. This is reflected in the aging dependence of the compliance curves (see Fig. 2) and should rationalize similar experimental findings of Siebenbürger *et al.* [7].

Since for the aged samples the transverse displacement maps indicate an inhomogeneous evolution of flow, one can expect that corresponding velocity profiles (which monitor the spatial dependence of the motion along the force direction) would also capture this behaviour. At

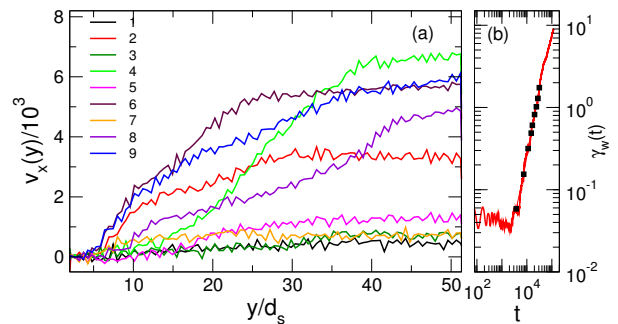


FIG. 3: (a) Velocity profiles during the onset of flow at $\sigma_0 = 0.1$ for a sample with age $t_{\text{age}} = 10^5$, averaged for $\Delta t = 498$, starting from different time-origins t_0 (labelled in sequence). (b) For the same trajectory, $\gamma_w(t)$ with the black squares marking the different t_0 .

the same imposed stress ($\sigma_0 = 0.1$), we show such velocity profiles in Fig. 3(a) for a trajectory sampled from the ensemble with $t_{\text{age}} = 10^5$. Since instantaneous profiles are too noisy, we average velocity profiles over short intervals in time ($\Delta t = 498$) starting at different points in time (t_0) after the imposition of the stress. In Fig. 3(b), we plot the evolution of the wall-strain $\gamma_w(t)$ for this trajectory and the different t_0 are marked on the curve; they correspond to the time-scales when the material “breaks” into flow. We see that, during these times, the velocity profiles fluctuate quite a lot, with signatures of intermittent flow (i.e. existence of little or no flow at some time instances, interspersed with bursts of flow) as well as the existence of band-like profiles (co-existence of regions of no-flow with more mobile regions). These transient heterogeneities in the velocity profiles, while in agreement with the observation in gels [5], reflect a more complex motion in flow direction.

Next, mobility maps are used to clarify the origin of the non-monotonicity in $\delta\gamma_w(t)$. For samples aged to $t_{\text{age}} = 10^5$, we study the dynamics for the independent trajectories evolving for $\sigma_0 = 0.092$. In Fig. 4(a), eight maps, calculated at $t = 42745$, from this ensemble are shown; the time of measurement is marked by an arrow in Fig. 4(b), which shows $\delta\gamma_w(t)$ for the entire ensemble. From map-to-map, one clearly sees that the local mobility is spatially different, with the occurrence of varying degrees of localization (or even the absence of it). Thus, this implies that even though all these confined samples have the same age, the local response to an imposed stress differs from one to the other, depending upon the initial state. Within an ensemble, the varying degree of fluidization indicates a distribution of time-scales for complete fluidization of each initial state; and this variation is macroscopically captured within $\delta\gamma_w(t)$. The increasing peak height of $\delta\gamma_w(t)$ with decreasing σ_0 (Fig. 1b) implies that this distribution becomes increasingly broad, which we can also see in the following way. For each σ_0 , we calculate the distribution of time-scale at which a strain of

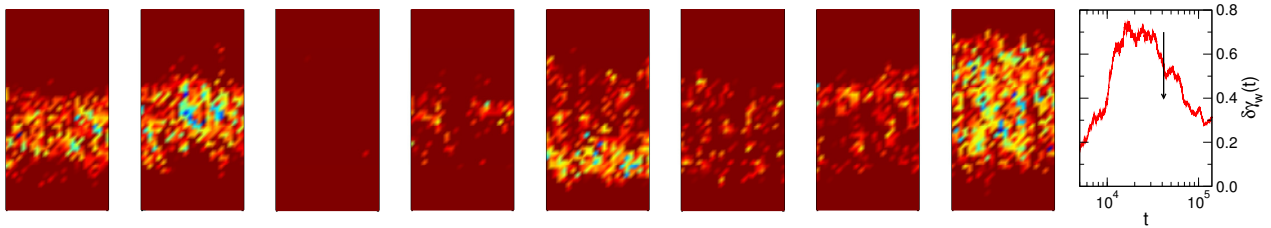


FIG. 4: For samples at $t_{\text{age}} = 10^5$ (left to right), the first eight panels show displacement maps for different trajectories at a fixed time $t = 42745$ for $\sigma_0 = 0.092$, indicating the variation in response of different samples at same t_{age} . Colorbar same as Fig. 2. (Last panel) $\delta\gamma_w(t)$ for the corresponding ensemble, with the arrow indicating the time of measurement.

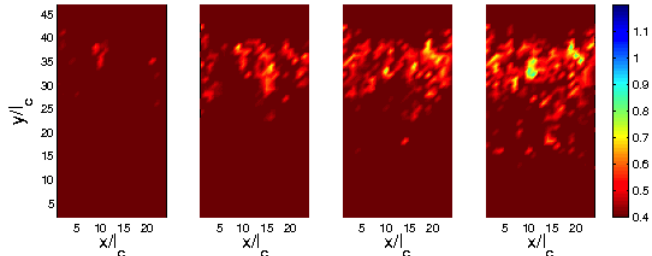


FIG. 5: For $\sigma = 0.08$, displacement maps along a single trajectory from the $t_{\text{age}} = 10^4$ ensemble. Measurements are done at $t = 10790, 25730, 92960, 251905$ (from left to right)

0.3 is reached for the set of m trajectories; the normalised variance (Γ) of this distribution is seen to increase with decreasing σ_0 (see Fig. 1(d) for the data corresponding to the ensemble with $t_{\text{age}} = 10^4$).

Finally, we investigate the local dynamics during the power-law creep for $\sigma_0 = 0.080$ (Fig. 5). Note that the local non-affine motion is extremely slow; even at $t = 10790$ (first panel on the left), only a few faint spots of significant displacements ($\mu_{lm}(t) > 0.5 d_s$) are seen. As time progresses, these spots expand into larger patches ($t = 25730$). By $t = 92960$, we see that these patches form a shear-band-like structure and this remains persistent till the end of our observation ($t = 251905$). In the rest of the system, even at such long time-scales, the mobility is comparably negligible. Thus transverse growth of mobilities seems to be impeded here, which makes the localisation long-lived (unlike when $\sigma > \sigma_d$).

In conclusion, using numerical simulations, we have demonstrated the existence of spatially heterogeneous dynamics during the onset of flow under imposed stress. The degree of heterogeneity and its lifetime increases with decreasing stress; and therefore creep flow (characterized by a power-law dependence of strain on time) is associated with long-lived shear-bands. It is to be noted that in most studies till now [30–35], shear-banding has been studied during steady flow, when an external shear-rate is imposed. In contrast, we use stress as a control parameter and thus we are able to investigate flow regimes both above and below yield stress. There, we see

the existence of such dynamical heterogeneities and their increasing lifetimes. Further, by studying this transient flow [36] from a quiescent glass, we can also check the role of aging (the history of which would be lost once the system is in steady flow). The evidence of the spatiotemporal heterogeneity that we put forth should also stimulate the development of theoretical models which can predict such fluctuations. Till now, most rheological models [7, 37, 38] predicting creep flows of various forms do not provide such scenarios. In that aspect, the non-local fluidity model [11] seems promising; however, the temporal evolution of spatial patterns of local fluidity, as the material starts flowing, needs to be worked out. Only recently, a more spatial version of the SGR model predicted that creep flow is associated with shear-banded velocity profiles [39] and our simulations confirm that.

Thus, even for a simple planar Couette flow geometry, a complex response is observed during the yielding of glasses. Further studies are necessary to clarify how this transient behaviour connects to creep observed in uniaxial tensile studies of metallic [40] and polymeric [41–43] glasses. For soft amorphous materials, while more local measurements are necessary from experiments, simulations can also explore the yielding response for inhomogeneous stress fields [44].

We thank L. Berthier, L. Bocquet, T. Divoux, S. Egelhaaf, W. Kob, M. Laurati, and T. Voigtmann for useful discussions. We acknowledge financial support by the German DFG, project No. SFB TR 6/A5, and computing time at the NIC Jülich.

-
- [1] D. Bonn and M. M. Denn, *Science* **324**, 1401 (2009).
 - [2] R. G. Larson, *The Structure and Rheology of Complex Fluids* (Oxford University Press, Oxford, 1998).
 - [3] P. C. F. Moller, A. Fall, and D. Bonn, *EPL* **87**, 38004 (2009).
 - [4] M. Laurati, S. U. Egelhaaf, and G. Petekidis, *J. Rheol.* **55**, 673 (2011).
 - [5] T. Divoux, C. Barentin, and S. Manneville, *Soft Matter* **7**, 8409 (2011).
 - [6] T. Divoux, D. Tamarii, C. Barentin, and S. Manneville, *Phys. Rev. Lett.* **104**, 208301 (2010).

- [7] M. Siebenbürger, M. Ballauff, and T. Voigtmann, Phys. Rev. Lett. **108**, 255701 (2012).
- [8] A. Tanguy, F. Leonforte, and J.-L. Barrat, Eur. Phys. J. E **20**, 355 (2006).
- [9] C. E. Maloney and A. Lemaitre, Phys. Rev. E **74**, 016118 (2006).
- [10] N. Koumakis, M. Laurati, S. U. Egelhaaf, J. F. Brady, and G. Petekidis, Phys. Rev. Lett. **108**, 098303 (2012).
- [11] L. Bocquet, A. Colin, and A. Ajdari, Phys. Rev. Lett. **103**, 036001 (2009).
- [12] J. Goyon, A. Colin, G. Ovarlez, A. Ajdari, and L. Bocquet, Nature **454**, 84 (2008); J. Goyon, A. Colin, and L. Bocquet, Soft Matter **6**, 2668 (2010).
- [13] P. Jop, V. Mansard, P. Chaudhuri, L. Bocquet, and A. Colin, Phys. Rev. Lett. **108**, 148301 (2012).
- [14] P. Chaudhuri, V. Mansard, A. Colin, and L. Bocquet, Phys. Rev. Lett. **109**, 036001 (2012).
- [15] A. Lemaitre and C. Caroli, Phys. Rev. Lett. **103**, 065501 (2009); J. Chattoraj, C. Caroli, and A. Lemaitre, Phys. Rev. Lett. **105**, 266001 (2010).
- [16] S. Karmakar, E. Lerner, and I. Procaccia, Phys. Rev. E **82**, 055103(R) (2010).
- [17] V. B. Nguyen, T. Darnige, A. Bruand, and E. Clement, Phys. Rev. Lett. **107**, 138303 (2011).
- [18] A. Amon, V. B. Nguyen, A. Bruand, J. Crassous, and E. Clement, Phys. Rev. Lett. **108**, 135502 (2012).
- [19] E. N. da C. Andrade, Proc. R. Soc. A **84**, 1 (1910).
- [20] D. W. Coffin, *Advances in Paper Science and Technology*, ed. S. J. I. Anson (FRC, Lancashire, 2005), p. 651.
- [21] F. R. N. Nabarro and F. De Villiers, *Physics of Creep and Creep-Resistant Alloys* (Taylor and Francis, London, 1995).
- [22] J. Rosti, J. Koivisto, L. Laurson, and M. J. Alava, Phys. Rev. Lett. **105**, 100601 (2010); L. Laurson, J. Rosti, J. Koivisto, A. Miksic, and M. J. Alava, J. Stat. Mech. P07002 (2011).
- [23] J. Zausch and J. Horbach, EPL **88**, 60001 (2009); J. Zausch, J. Horbach, M. Laurati, S. U. Egelhaaf, J. M. Brader, T. Voigtmann, and M. Fuchs, J. Phys.: Condens. Matter **20**, 404210 (2008).
- [24] D. Winter, J. Horbach, P. Virnau, and K. Binder, Phys. Rev. Lett. **108**, 028303 (2012).
- [25] C. P. Lowe, Europhys. Lett. **47**, 145 (1999); E. A. Koopman and C. P. Lowe, J. Chem. Phys. **124**, 204103 (2006).
- [26] F. Varnik, L. Bocquet, and J.-L. Barrat, J. Chem. Phys. **120**, 2788 (2004).
- [27] The dynamic yield stress (σ_d) was estimated via constant shear-rate ($\dot{\gamma}_0$) simulations [34]. Measured shear stress σ is fitted with the Herschel-Bulkley function $\sigma = \sigma_d[1 + (\dot{\gamma}_0/\dot{\gamma}_c)^n]$ to obtain σ_d .
- [28] L. Berthier, Physics **4**, 42 (2011).
- [29] Y. Shi and M. L. Falk, Phys. Rev. Lett. **95**, 095502 (2005).
- [30] J.-L. Barrat and A. Lemaitre, Dynamical Heterogeneities in Glasses, Colloids, and Granular Materials, Chap. 8 (Oxford University Press, Oxford, 2011); *arXiv:1009.5774*.
- [31] P. Schall and M. van Hecke, Ann. Rev. Fluid Mech. **42**, 67 (2010).
- [32] R. Besseling, L. Isa, P. Ballesta, G. Petekidis, M. E. Cates, and W. C. K. Poon, Phys. Rev. Lett. **105**, 268301 (2010).
- [33] G. Ovarlez, S. Rodts, X. Chateau, and P. Coussot, Rheol. Acta **48**, 831 (2009).
- [34] F. Varnik, L. Bocquet, J.-L. Barrat, and L. Berthier, Phys. Rev. Lett. **90**, 095702 (2003).
- [35] P. Chaudhuri, L. Berthier, and L. Bocquet, Phys. Rev. E **85**, 021503 (2012).
- [36] R. L. Moorcroft, M. E. Cates, and S. M. Fielding, Phys. Rev. Lett. **106**, 055502 (2011).
- [37] S. M. Fielding, P. Sollich, and M. E. Cates, J. Rheol. **44**, 323 (2000).
- [38] C. Derec, A. Ajdari, and F. Lequeux, Eur. Phys. J. E **4**, 355 (2001).
- [39] R. L. Moorcroft and S. M. Fielding, Phys. Rev. Lett. **110**, 086001 (2013).
- [40] M. Schwabe, D. Bedorf, and K. Samwer, Eur. Phys. J. E **34**, 91 (2011).
- [41] H. N. Lee, K. Paeng, S. F. Swallen, and M. D. Ediger, Science **323**, 231 (2009).
- [42] R. A. Riggleman, H.-N. Lee, M. D. Ediger, and J. J. de Pablo, Phys. Rev. Lett. **99**, 215501 (2007).
- [43] M. Warren and J. Rottler, Phys. Rev. Lett. **104**, 205501 (2010).
- [44] P. Chaudhuri and J. Horbach, in preparation.